Supporting Information for:

# Mathematical models incorporating a multi-stage cell cycle explain synchronisation in proliferation experiments

S. T. Vittadello, S. W. McCue, G. Gunasingh, N. K. Haass, M. J. Simpson

*February 19, 2019*

# Contents

# 1 Experimental

Here we provide further details of the experimental set-up we use for the three melanoma cell lines employed in our cell proliferation experiments.

## 1.1 Cell culture

The human melanoma cell lines C8161 (kindly provided by Mary Hendrix, Chicago, IL, USA), WM983C and 1205Lu (both kindly provided by Meenhard Herlyn, Philadelphia, PA, USA) were genotypically characterised [1–4], grown as described [5] (using 4% fetal bovine serum instead of 2%), and authenticated by STR fingerprinting (QIMR Berghofer Medical Research Institute, Herston, Australia).

## 1.2 Fluorescent ubiquitination-based cell cycle indicator (FUCCI)

To generate stable melanoma cell lines expressing the FUCCI constructs, mKO2-hCdt1 (30-120) and mAG-hGem (1-110) [6] were subcloned into a replication-defective, self-inactivating lentiviral expression vector system as previously described [5]. The lentivirus was produced by co-transfection of human embryonic kidney 293T cells. High-titer viral solutions for mKO2-hCdt1 (30/120) and mAG-hGem (1/110) were prepared and used for co-transduction into the melanoma cell lines, and subclones were generated by single cell sorting [7–9].

# 2 Image processing and analysis

The microscopy data consist of multi-channel time-series stacks which are processed and analysed automatically with Fiji/ImageJ and MATLAB as described below.

## 2.1 Preprocessing

To maximise the accuracy in identifying particles, which in our case are cell nuclei, we enhance the quality of the microscopy images using ImageJ as follows.

1. Import the time-series stack with the Bio-Formats Importer plugin, splitting the red and green channels.
2. Apply five iterations of Subtract Background with rolling-ball radius of 5 pixels.
3. Apply Enhance Contrast with the Equalize Histogram option selected.
4. Apply the Gaussian Blur filter with sigma = 1.

## 2.2 Segmentation

We now identify the particles in the processed images using ImageJ.

1. Apply Auto-thresholding using the Yen method, selecting the option to 'calculate the threshold for each image'.
2. The resulting binary images are then refined by applying:
   (a) Watershed;
   (b) Fill Holes;
   (c) Open, with iterations = 10 and count = 5;
   (d) Watershed.

## 2.3 Analysis

For every image in the segmented binary time-series stacks we count the number of particles in each of the red and green channels using ImageJ. We then use MATLAB to determine which particles are yellow.

1. For each of the red and green channels, apply Analyze Particles in ImageJ with sizes in the range 5–$\infty$ pixels$^2$ and the option 'limit to threshold' selected. Output the stack position and the centroid of every particle in each channel.

2. We now need to determine which particles are red, yellow or green. A particle is red if it appears in the red channel, and there is no corresponding particle in the green channel. Similarly, a particle is green if it appears in the green channel, and there is no corresponding particle in the red channel. A particle is then yellow if it appears in both the red and green channels. Identifying whether a particle appears in both the red and green channels is complicated by the possible alteration of the shape of the particle during image processing. While we process every image in exactly the same way, the original microscopy images may have different signal-to-noise ratios between the red and green channels. Consequently, there may be a difference in the shape of a particle depending on which channel it is viewed, and thereby a difference in the centroid in each channel. We therefore use MATLAB to determine which particles are red, yellow or green, using the stack position and centroid of each particle, as follows.

   (a) We first find the yellow particles using the stack position and centroid of each particle, so choose a particle, in turn, from the red channel.

   (b) Search the green channel for a corresponding particle such that the Euclidean distance between the centroids of the two particles is not greater than 3 pixels, noting that the resolution of our images is 1.8150 $\mu$m pixel$^{-1}$. This distance allows for a location error of the centroids of the red and green particles, whereby the centroids may be translated up to one pixel from the original centroid of the yellow particle in the unprocessed images. Placing the original yellow centroid at the centre of a $3 \times 3$ grid of pixels, the red and green centroids from the processed images may be located at any of the nine pixels in the grid.

(c) Once all of the yellow particles are found, the red particles are all of the particles in the red channel which are not yellow. Similarly, the green particles are all of the particles in the green channel which are not yellow.

# 3 Parameterisation of the exponential model

To estimate the parameters of the exponential model Equation (1) when fitting the model solution to the experimental data for total number of cells, we use the the `fit` function and `exp1` model [10] in MATLAB. The parameter estimates, with 95% confidence intervals, are:

- **C8161 cell line - Figure 1(i)**

  $M(0) = 524.3$ $(515.1, 533.4)$ and $\lambda = 0.03504$ $\text{h}^{-1}$ $(0.03456, 0.03551)$.

- **WM983C cell line - Figure S2(e)**

  $M(0) = 247.7$ $(244.3, 251.2)$ and $\lambda = 0.02541$ $\text{h}^{-1}$ $(0.02501, 0.02581)$.

- **1205Lu cell line - Figure S3(e)**

  $M(0) = 215.9$ $(214.1, 217.7)$ and $\lambda = 0.01932$ $\text{h}^{-1}$ $(0.01907, 0.01958)$.

# 4 Parameterisation of the multi-stage mathematical model

Here we describe our methodology for estimating the parameters of the multi-stage mathematical model Equation (2) and fitting the model solution to the experimental data.

## 4.1 Method for parameter estimation

The multi-stage model requires specification of the number of stages, the transition rates from each stage to the successive stage, and the initial population in each stage. In this work, we aim to achieve the best fit of the model to our data while keeping the number of model parameters with distinct values to a minimum.

We partition the phases G1, eS and S/G2/M into the same number of stages, $S$. The mean durations of the phases G1, eS and S/G2/M are denoted by $L_r$, $L_y$ and $L_g$, respectively. The transition rates between successive stages are set equal within each phase to $S/L_r$ in G1, $S/L_y$ in eS and $S/L_g$ in S/G2/M. For each $i = 1, \ldots, S$ we denote the mean number of cells at time $t$ in stage $i$ of G1 as $R_i(t)$, of eS as $Y_i(t)$, and of

S/G2/M as $G_i(t)$. Therefore, $R(t) = \sum_{i=1}^{S} R_i(t)$, $Y(t) = \sum_{i=1}^{S} Y_i(t)$ and $G(t) = \sum_{i=1}^{S} G_i(t)$. The parameters that we need to estimate are the components of the vector

$$\mathbf{x} = [\, R_1(0) \,\ldots\, R_S(0) \quad Y_1(0) \,\ldots\, Y_S(0) \quad G_1(0) \,\ldots\, G_S(0) \quad L_r \quad L_y \quad L_g \,]. \tag{S1}$$

The parameters in Equation (S1) are either numbers of cells or phase durations, which are all non-negative, so we require our optimisation algorithm to accept bound constraints. To find estimates for these parameters we use the MATLAB nonlinear least-squares solver `lsqnonlin` [11] with the trust-region-reflective algorithm [12], which allows for bound constraints of the parameters. In the following, a dependent variable has the subscript 'model' or 'data' to distinguish between model and data values of the variable. With non-negative weights $w_2, \ldots, w_6$, we define the vector objective function

$$\mathbf{F}(\mathbf{x}) = [\, \mathbf{f}_1(\mathbf{x}) \; w_2\mathbf{f}_2(\mathbf{x}) \; w_3\mathbf{f}_3(\mathbf{x}) \; w_4\mathbf{f}_4(\mathbf{x}) \; w_5\mathbf{f}_5(\mathbf{x}) \; w_6\mathbf{f}_6(\mathbf{x}) \,] \tag{S2}$$

as the concatenation of the weight-scaled vectors

$$\mathbf{f}_1(\mathbf{x}) = \big[\, \big(Q_{\text{model}}(\mathbf{x}) - Q_{\text{data}}\big)(t_1) \quad \ldots \quad (Q_{\text{model}}(\mathbf{x}) - Q_{\text{data}})(t_n) \,\big], \tag{S3}$$

$$\mathbf{f}_2(\mathbf{x}) = \big[\, \big(R_{\text{model}}(\mathbf{x}) - R_{\text{data}}\big)(t_1) \quad \ldots \quad \big(R_{\text{model}}(\mathbf{x}) - R_{\text{data}}\big)(t_n) \,\big], \tag{S4}$$

$$\mathbf{f}_3(\mathbf{x}) = \big[\, \big(Y_{\text{model}}(\mathbf{x}) - Y_{\text{data}}\big)(t_1) \quad \ldots \quad \big(Y_{\text{model}}(\mathbf{x}) - Y_{\text{data}}\big)(t_n) \,\big], \tag{S5}$$

$$\mathbf{f}_4(\mathbf{x}) = \big[\, \big(G_{\text{model}}(\mathbf{x}) - G_{\text{data}}\big)(t_1) \quad \ldots \quad \big(G_{\text{model}}(\mathbf{x}) - G_{\text{data}}\big)(t_n) \,\big], \tag{S6}$$

$$\mathbf{f}_5(\mathbf{x}) = \big[\, \big(G_{\text{model}}(\mathbf{x}) - G_{\text{data}}\big)(t_n) \,\big], \tag{S7}$$

$$\mathbf{f}_6(\mathbf{x}) = \big[\, \mathcal{T} - L_r - L_y - L_g \,\big], \tag{S8}$$

where:

1. $Q_{\text{model}}(\mathbf{x})$ is the ratio of the number of cells in G1 to the number of cells in eS/S/G2/M, from the model solution;

2. $Q_{\text{data}}$ is the ratio of the number of cells in G1 to the number of cells in eS/S/G2/M, from the data;

3. $R_{\text{model}}(\mathbf{x})$, $Y_{\text{model}}(\mathbf{x})$ and $G_{\text{model}}(\mathbf{x})$ are the subpopulations of cells in G1, eS and S/G2/M, respectively, from the model solution;

4. $\mathcal{R}_{\text{data}}$, $\mathcal{Y}_{\text{data}}$ and $\mathcal{G}_{\text{data}}$ are the subpopulations of cells in G1, eS and S/G2/M, respectively, from the data;

5. $t_1 < \cdots < t_n$ are the data time points over 48 hours;

6. $\mathcal{T}$ is the cell cycle time.

The vector $\mathbf{f}_1$ is used to fit the model to the ratio data, and the vectors $\mathbf{f}_2, \ldots, \mathbf{f}_4$ are used to fit the model to the three subpopulations corresponding to G1, eS and S/G2/M. Preliminary results (not shown) indicate that it is not necessary to fit the model to the total population data as a good fit follows from fitting to the subpopulations. The vector $\mathbf{f}_5$ fits the model to the S/G2/M subpopulation data at the final time point, and the vector $\mathbf{f}_6$ constrains the estimated phase durations to sum to the expected cell cycle time.

Note that the weights in the objective function Equation (S2) are specified prior to optimising the estimates of the parameters in Equation (S1). The weights differ between cell lines in order to obtain the best fit of the model to each data set.

## 4.2 Specific estimated parameters

Here we provide the estimated parameters of the multi-stage model corresponding to Figure 1. We also provide parameter estimates for the model corresponding to data from the WM983C (Figure S2) and 1205Lu (Figure S3) cell lines.

### 4.2.1 C8161 cell line - Figure 1

The experimentally-determined mean cell cycle time for C8161 is approximately $\mathcal{T} = 18$ h [7]. We partition each cell cycle phase into $S = 18$ stages, giving a total of $k = 54$ stages for the complete cell cycle. In each phase

we set the first half of the stages, totalling 9 stages, to have equal numbers of cells, and the second half of the stages to have equal numbers of cells. We therefore only require a total of six distinct population parameters. The vector objective function is $\mathbf{F}(\mathbf{x}) = [\,\mathbf{f}_1(\mathbf{x})\ 10^{-4}\mathbf{f}_2(\mathbf{x})\ 10^{-4}\mathbf{f}_3(\mathbf{x})\ 10^{-4}\mathbf{f}_4(\mathbf{x})\ 10^{-3}\mathbf{f}_5(\mathbf{x})\,]$. Starting with the parameters $R_i(0) = Y_i(0) = G_i(0) = 0.5$ for $i = 1, \ldots, S$, and $L_r = L_y = L_g = 6$, we obtain the parameterisation

$$R_i(0) = \begin{cases} 15.48 & \text{for } i = 1, \ldots, 9, \\ 12.93 & \text{for } i = 10, \ldots, 18, \end{cases} \qquad Y_i(0) = \begin{cases} 12.94 & \text{for } i = 1, \ldots, 9, \\ 5.41 & \text{for } i = 10, \ldots, 18, \end{cases}$$

$$G_i(0) = \begin{cases} 2.51 & \text{for } i = 1, \ldots, 9, \\ 3.48 & \text{for } i = 10, \ldots, 18, \end{cases} \qquad \begin{aligned} L_r &= 6.14 \text{ h}, \\ L_y &= 7.43 \text{ h}, \\ L_g &= 4.42 \text{ h}. \end{aligned} \tag{S9}$$

All parameter estimates given in this document are presented to two decimal places. Note that $L_r + L_y + L_g = 17.99$ h, in good agreement with the observed cell cycle time of 18 h.

#### 4.2.2 C8161 cell line, different numbers of stages - Figure S1

In Figure S1 we compare solutions of the multi-stage model for $S = 2$, 6, 10 and 14 stages per phase, with the ratio $Q_{\text{data}}$. In fitting the model solution we use the same parameters as for Figure 1, except the number of stages differ. For each number of stages, in each phase we set the first half of the stages to have equal numbers of cells and the second half of the stages to have equal numbers of cells, so that we therefore only require a total of 6 distinct population parameters. Starting with the parameters $R_i(0) = Y_i(0) = G_i(0) = 0.5$

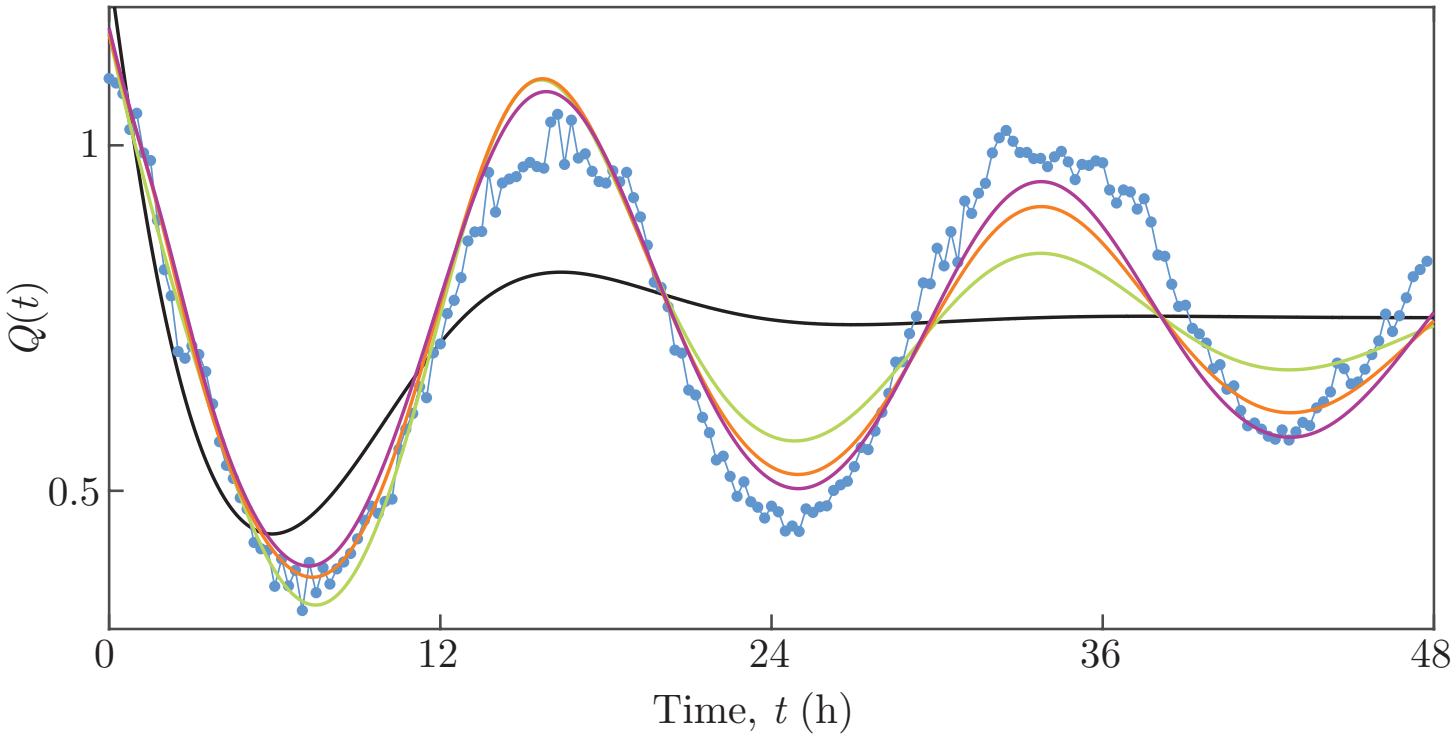


**Figure S1: $Q(t)$ for C8161 experimental data and multi-stage model solutions with different numbers of stages.** Experimental data are shown as discs and the model solutions as curves. The model solutions with 2, 6, 10 and 14 stages are the black, green, orange and purple curves, respectively.

for $i = 1, \ldots, S$, and $L_r = L_y = L_g = 6$, the parameterisation for $S = 14$ is

$$R_i(0) = \begin{cases} 17.89 & \text{for } i = 1, \ldots, 9, \\ 18.62 & \text{for } i = 10, \ldots, 18, \end{cases} \qquad Y_i(0) = \begin{cases} 16.28 & \text{for } i = 1, \ldots, 9, \\ 6.77 & \text{for } i = 10, \ldots, 18, \end{cases}$$

$$G_i(0) = \begin{cases} 2.39 & \text{for } i = 1, \ldots, 9, \\ 5.78 & \text{for } i = 10, \ldots, 18, \end{cases} \qquad \begin{aligned} L_r &= 6.17 \text{ h}, \\ L_y &= 7.27 \text{ h}, \\ L_g &= 4.64 \text{ h}, \end{aligned} \tag{S10}$$

the parameterisation for $S = 10$ is

$$R_i(0) = \begin{cases} 16.60 & \text{for } i = 1, \ldots, 9, \\ 33.58 & \text{for } i = 10, \ldots, 18, \end{cases} \qquad Y_i(0) = \begin{cases} 20.81 & \text{for } i = 1, \ldots, 9, \\ 9.61 & \text{for } i = 10, \ldots, 18, \end{cases}$$

$$G_i(0) = \begin{cases} 0 & \text{for } i = 1, \ldots, 9, \\ 12.81 & \text{for } i = 10, \ldots, 18, \end{cases} \qquad \begin{aligned} L_r &= 6.22 \text{ h}, \\ L_y &= 7.06 \text{ h}, \\ L_g &= 4.92 \text{ h}, \end{aligned} \tag{S11}$$

the parameterisation for $S = 6$ is

$$R_i(0) = \begin{cases} 16.42 & \text{for } i = 1, \ldots, 9, \\ 66.47 & \text{for } i = 10, \ldots, 18, \end{cases} \qquad Y_i(0) = \begin{cases} 44.97 & \text{for } i = 1, \ldots, 9, \\ 0 & \text{for } i = 10, \ldots, 18, \end{cases}$$

$$G_i(0) = \begin{cases} 0 & \text{for } i = 1, \ldots, 9, \\ 26.34 & \text{for } i = 10, \ldots, 18, \end{cases} \qquad \begin{aligned} L_r &= 6.28 \text{ h}, \\ L_y &= 6.81 \text{ h}, \\ L_g &= 5.21 \text{ h}, \end{aligned} \tag{S12}$$

and the parameterisation for $S = 2$ is

$$R_i(0) = \begin{cases} 195.22 & \text{for } i = 1, \ldots, 9, \\ 107.41 & \text{for } i = 10, \ldots, 18, \end{cases} \qquad Y_i(0) = \begin{cases} 241.05 & \text{for } i = 1, \ldots, 9, \\ 0 & \text{for } i = 10, \ldots, 18, \end{cases}$$

$$G_i(0) = \begin{cases} 0 & \text{for } i = 1, \ldots, 9, \\ 0 & \text{for } i = 10, \ldots, 18, \end{cases} \qquad \begin{aligned} L_r &= 6.91 \text{ h}, \\ L_y &= 7.11 \text{ h}, \\ L_g &= 5.79 \text{ h}. \end{aligned} \tag{S13}$$

The corresponding solutions of the multi-stage model are shown in Figure S1.

Considering parameterisations of the model whereby in each phase we set the first half of the stages to have

equal numbers of cells and the second half of the stages to have equal numbers of cells, the oscillations decay at a faster rate for a smaller number of stages per phase. A higher number of stages produces a hypoexponential distribution with lower variance, resulting in oscillations which are sustained for longer. Consequently, fewer than 18 stages per phase results in a model solution with a poorer fit.

#### 4.2.3 WM983C cell line - Figure S2

The experimentally-determined mean cell cycle time for WM983C is $\mathcal{T} = 27$ h [7]. We partition each cell cycle phase into $S = 10$ stages, giving a total of $k = 30$ stages for the complete cell cycle. From the start of each phase we set every 2 successive stages to have equal numbers of cells. We therefore only require a total of 15 distinct population parameters. The vector objective function is $\mathbf{F}(\mathbf{x}) = [\,\mathbf{f}_1(\mathbf{x})\;\; 10^{-3}\mathbf{f}_2(\mathbf{x})\;\; 10^{-3}\mathbf{f}_3(\mathbf{x})\;\; 10^{-3}\mathbf{f}_4(\mathbf{x})\;\; 10\,\mathbf{f}_6(\mathbf{x})$ Starting with the parameters

$$R_i(0) = \begin{cases} 0 & \text{for } i = 1, 2, \\ 0 & \text{for } i = 3, 4, \\ 29.23 & \text{for } i = 5, 6, \\ 19.66 & \text{for } i = 7, 8, \\ 0 & \text{for } i = 9, 10, \end{cases} \qquad Y_i(0) = \begin{cases} 33.02 & \text{for } i = 1, 2, \\ 0 & \text{for } i = 3, 4, \\ 0 & \text{for } i = 5, 6, \\ 0 & \text{for } i = 7, 8, \\ 0 & \text{for } i = 9, 10, \end{cases}$$

$$G_i(0) = \begin{cases} 11.04 & \text{for } i = 1, 2, \\ 0 & \text{for } i = 3, 4, \\ 4.29 & \text{for } i = 5, 6, \\ 24.41 & \text{for } i = 7, 8, \\ 0 & \text{for } i = 9, 10, \end{cases} \qquad \begin{aligned} L_r &= 10.28 \text{ h}, \\ L_y &= 3.87 \text{ h}, \\ L_g &= 12.85 \text{ h}, \end{aligned} \tag{S14}$$

we obtain the same parameterisation Equation (S14). Note that $L_r + L_y + L_g = 27.00$ h, in good agreement with the observed cell cycle time of 27 h.

#### 4.2.4 1205Lu cell line - Figure S3

The experimentally-determined mean cell cycle time for 1205Lu is $\mathcal{T} = 36$ h [7]. We partition each cell cycle phase into $S = 20$ stages, giving a total of $k = 60$ stages for the complete cell cycle. From the start of each phase we set every 5 successive stages to have equal numbers of cells. We therefore only require a total of 12 distinct population parameters. The vector objective function is $\mathbf{F}(\mathbf{x}) = [\,\mathbf{f}_1(\mathbf{x})\ \ 10^{-2}\mathbf{f}_2(\mathbf{x})\ \ 10^{-2}\mathbf{f}_3(\mathbf{x})\ \ 10^{-2}\mathbf{f}_4(\mathbf{x})\ \ 0.5\,\mathbf{f}_6(\mathbf{x})$ Starting with the parameters

$$R_i(0) = \begin{cases} 0.27 \quad \text{for } i = 1, \ldots, 5, \\ 0 \quad \text{for } i = 6, \ldots, 10, \\ 21.78 \quad \text{for } i = 11, \ldots, 15, \\ 0 \quad \text{for } i = 16, \ldots, 20, \end{cases} \qquad Y_i(0) = \begin{cases} 4.73 \quad \text{for } i = 1, \ldots, 5, \\ 5.39 \quad \text{for } i = 6, \ldots, 10, \\ 0 \quad \text{for } i = 11, \ldots, 15, \\ 2.49 \quad \text{for } i = 16, \ldots, 20, \end{cases}$$

$$G_i(0) = \begin{cases} 3.15 \quad \text{for } i = 1, \ldots, 5, \\ 5.17 \quad \text{for } i = 6, \ldots, 10, \\ 2.08 \quad \text{for } i = 11, \ldots, 15, \\ 0.45 \quad \text{for } i = 16, \ldots, 20, \end{cases} \qquad \begin{aligned} L_r &= 20.97 \text{ h}, \\ L_y &= 10.07 \text{ h}, \\ L_g &= 10.52 \text{ h}, \end{aligned} \tag{S15}$$

we obtain the parameterisation

$$R_i(0) = \begin{cases} 0 \quad \text{for } i = 1, \ldots, 5, \\ 13.79 \quad \text{for } i = 6, \ldots, 10, \\ 5.73 \quad \text{for } i = 11, \ldots, 15, \\ 4.19 \quad \text{for } i = 16, \ldots, 20, \end{cases} \qquad Y_i(0) = \begin{cases} 9.39 \quad \text{for } i = 1, \ldots, 5, \\ 0 \quad \text{for } i = 6, \ldots, 10, \\ 0 \quad \text{for } i = 11, \ldots, 15, \\ 5.04 \quad \text{for } i = 16, \ldots, 20, \end{cases}$$

$$G_i(0) = \begin{cases} 2.31 \quad \text{for } i = 1, \ldots, 5, \\ 0 \quad \text{for } i = 6, \ldots, 10, \\ 3.52 \quad \text{for } i = 11, \ldots, 15, \\ 0.63 \quad \text{for } i = 16, \ldots, 20, \end{cases} \qquad \begin{aligned} L_r &= 19.61 \text{ h}, \\ L_y &= 7.99 \text{ h}, \\ L_g &= 10.76 \text{ h}, \end{aligned} \tag{S16}$$

Note that $L_r + L_y + L_g = 38.36$ h, in good agreement with the observed cell cycle time of 36 h.

# 5 Experimental data and multi-stage model solutions for the WM983C and 1205Lu cell lines.

Figures S2 and S3 provide comparisons of the experimental data and solutions of the multi-stage model Equation (2) for the WM983C and 1205Lu cell lines, similar to Figure 1 for the C8161 cell line.

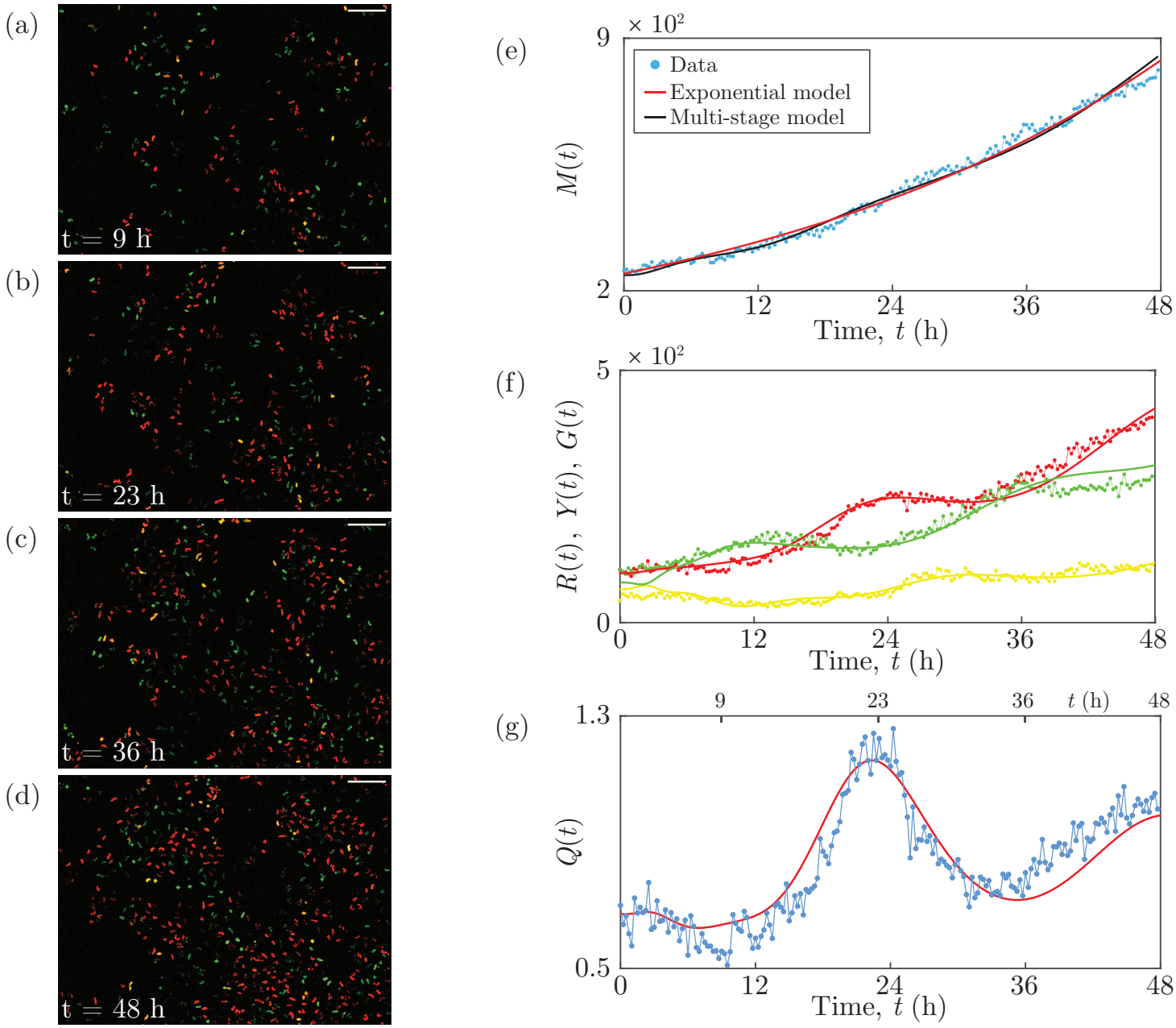


**Figure S2: WM983C experimental data and multi-stage model solution.** (a)–(d) Images of a proliferation assay with FUCCI-WM983C cells. Scale bar 200 $\mu$m. (e) $M(t)$. (f) $R(t)$, $Y(t)$ and $G(t)$. (g) $Q(t)$. Experimental data are shown as discs and the model solutions as curves.

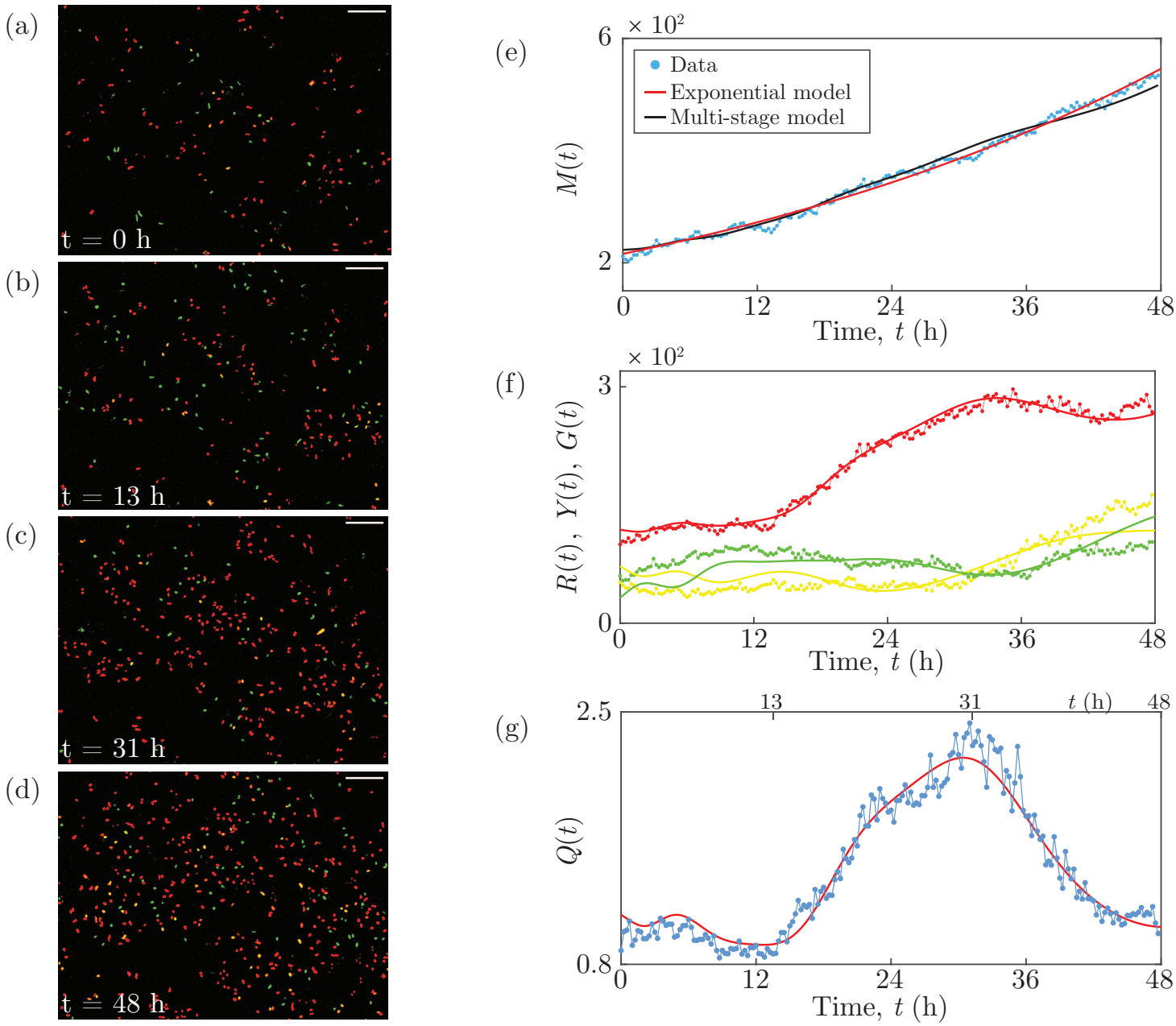


**Figure S3: 1205Lu experimental data and multi-stage model solution.** (a)–(d) Images of a proliferation assay with FUCCI-1205Lu cells. Scale bar 200 $\mu$m. (e) $M(t)$. (f) $R(t)$, $Y(t)$ and $G(t)$. (g) $Q(t)$. Experimental data are shown as discs and the model solutions as curves.

# 6 All experimental data

Here we provide all of our new experimental data in the form of the total number of cells $M(t)$ and the ratio $Q(t)$ of the number of cells in G1 to the number of cells in eS/S/G2/M. These data are obtained from the three cell lines C8161, WM983C and 1205Lu, and four independent experiments. In Experiments 1–3 we use one well of a 24-well plate, and in Experiment 4 we use two wells of a 24-well plate. From each well we obtain six time-series stacks at different positions.

The population growth appears to be exponential in every case. The data show that partially synchronous populations are present in every experiment. Further, in a given well, the six different positions can exhibit different degrees of synchronisation, and the synchronisation can be out of phase between the different wells.

Note that for some of the data there are a couple of consecutive time points which show a much higher total number of cells than expected, and a corresponding lower ratio in the ratio data. This is due to a large decrease in the signal-to-noise ratio in the green channel at these time points. The specific cause of this is unknown, however fluorescence microscopy is subject to such variations in the signal-to-noise ratio at times. As there is such a large reduction in the signal-to-noise ratio, it is not possible to reduce the unwanted noise without compromising the signal quality.

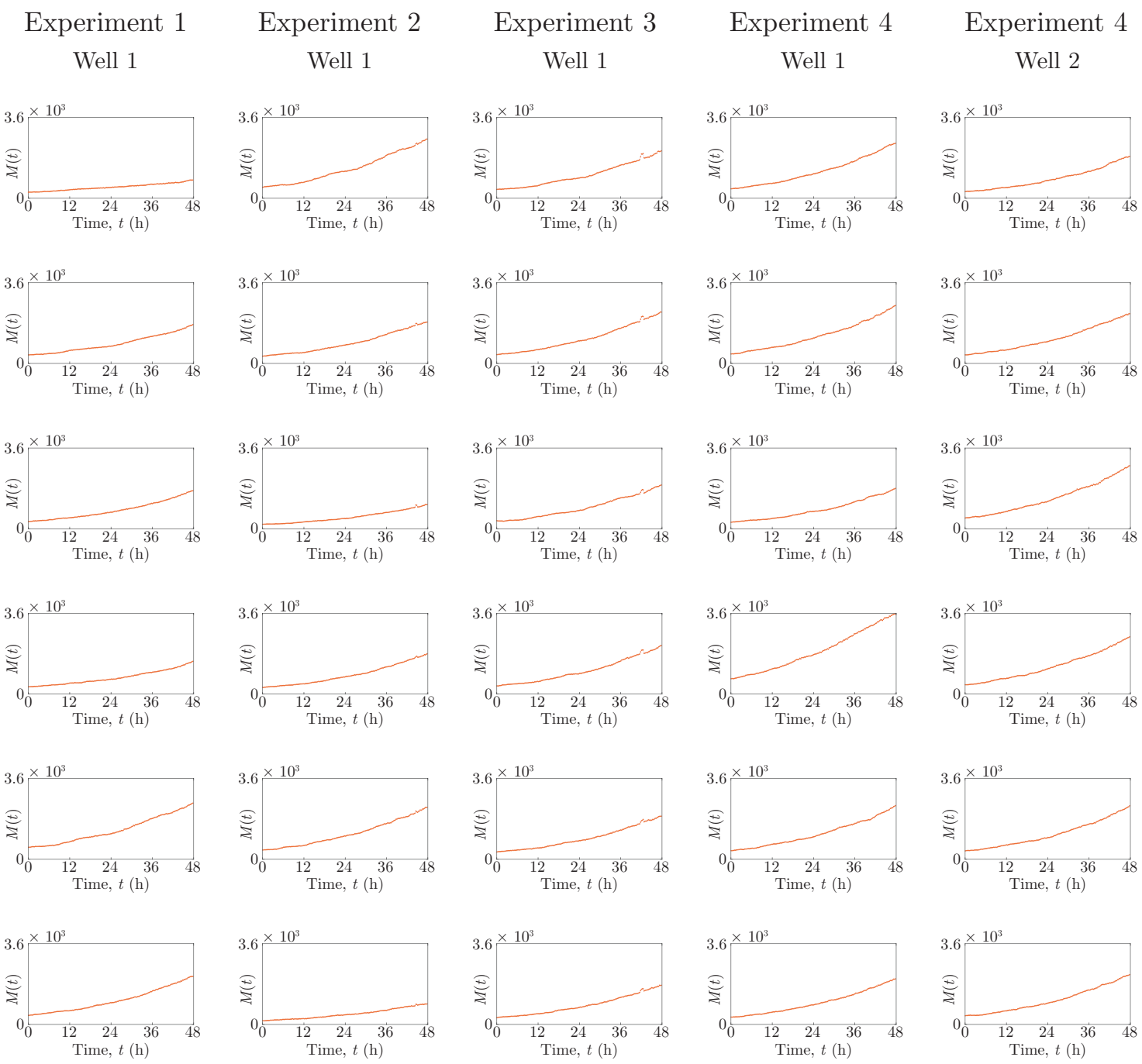


**Figure S4: C8161 experimental data.** Total number of cells $M(t)$.

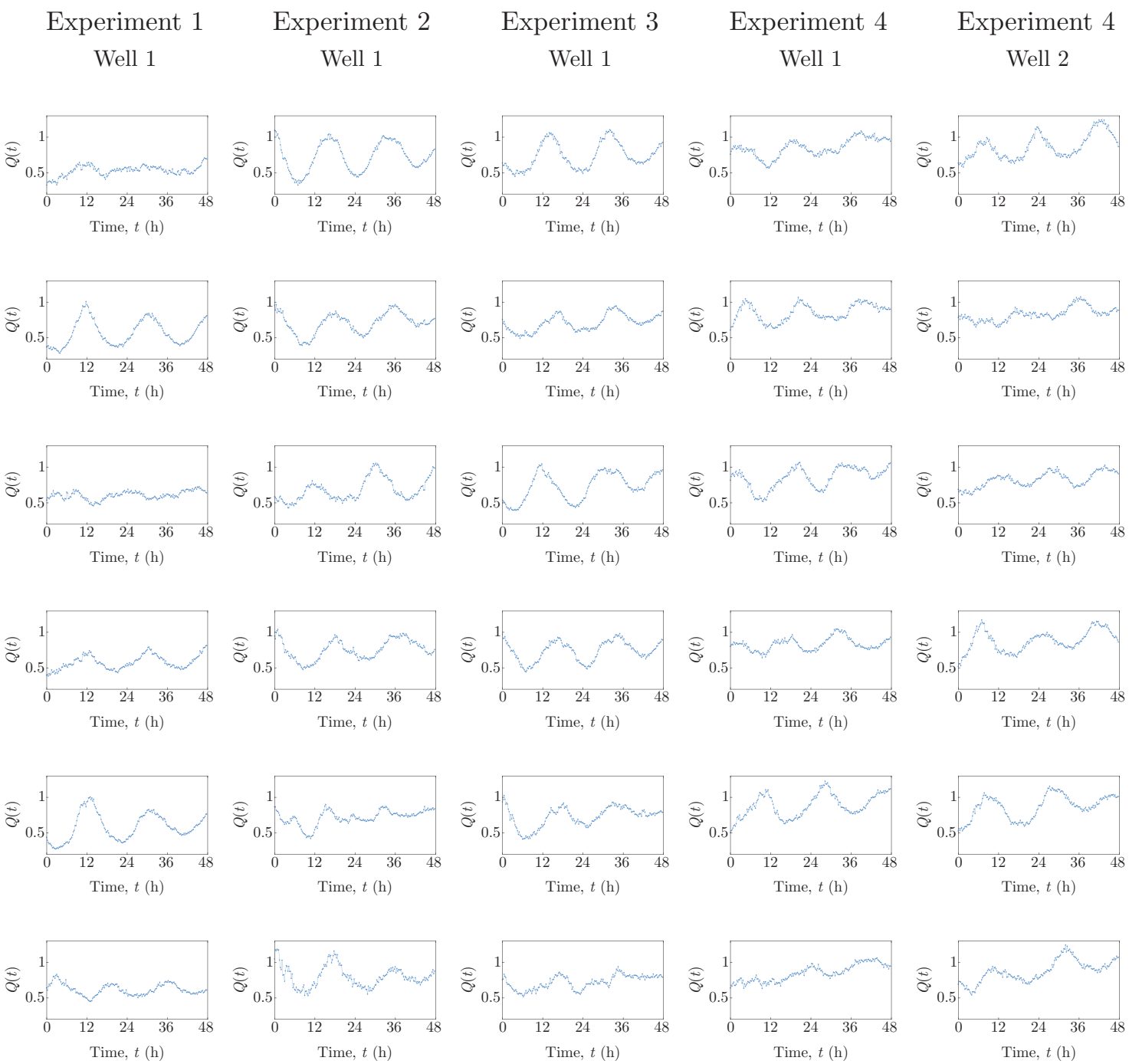


**Figure S5: C8161 experimental data.** Ratio $Q(t)$ of the number of cells in G1 to the number of cells in eS/S/G2/M.

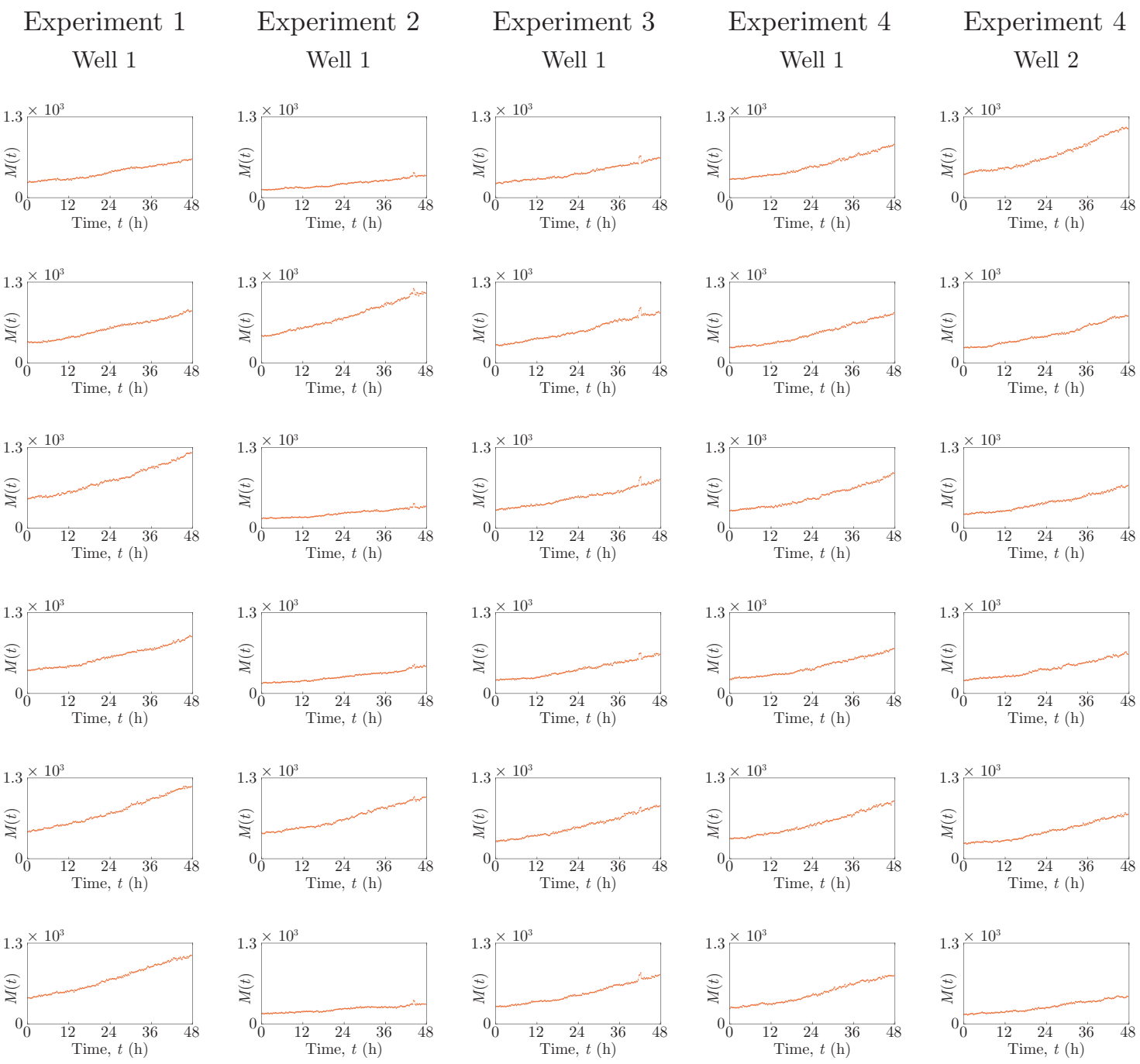


**Figure S6: WM983C experimental data.** Total number of cells $M(t)$.

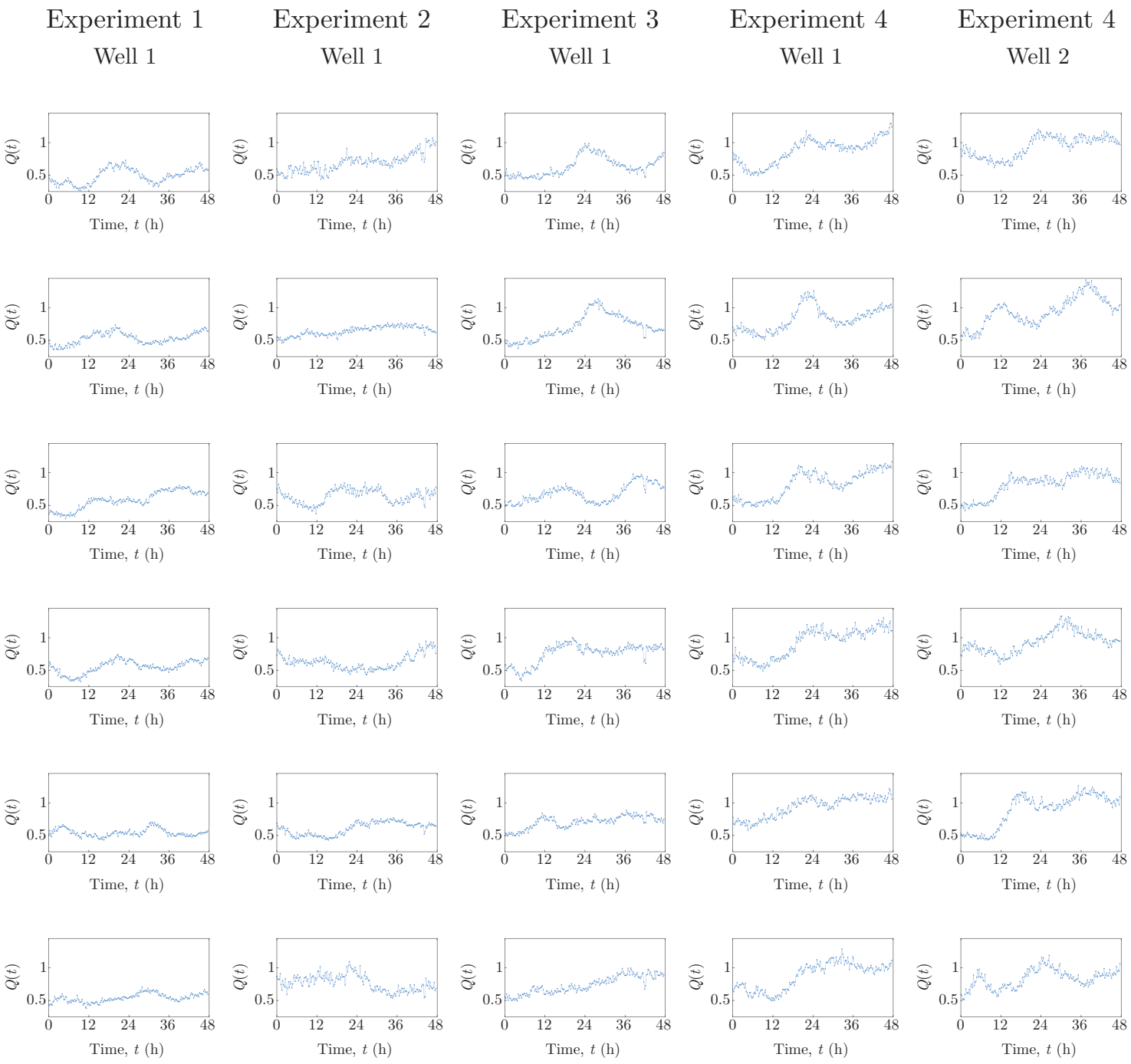


**Figure S7: WM983C experimental data.** Ratio $Q(t)$ of the number of cells in G1 to the number of cells in eS/S/G2/M.

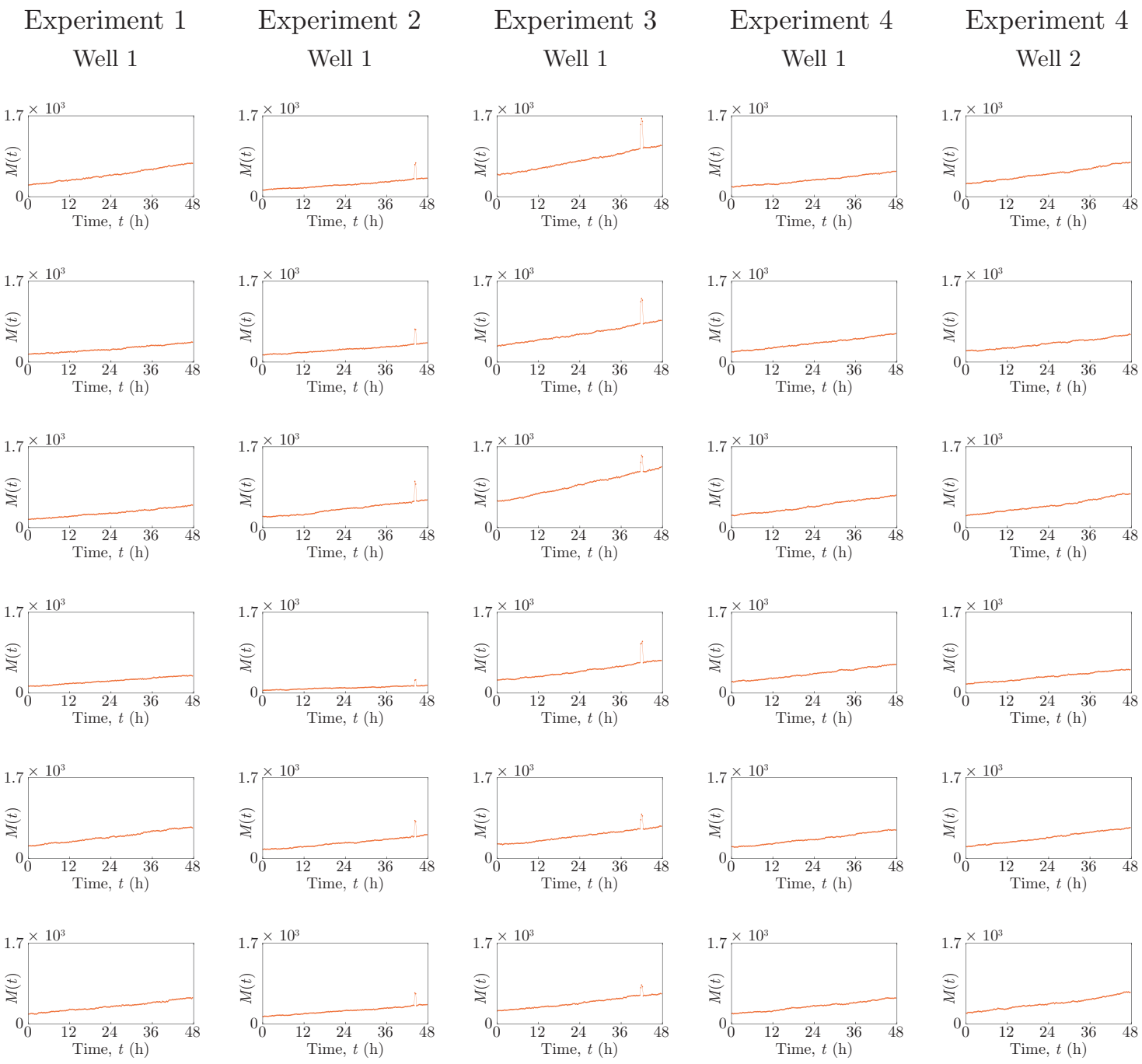


**Figure S8: 1205Lu experimental data.** Total number of cells $M(t)$.

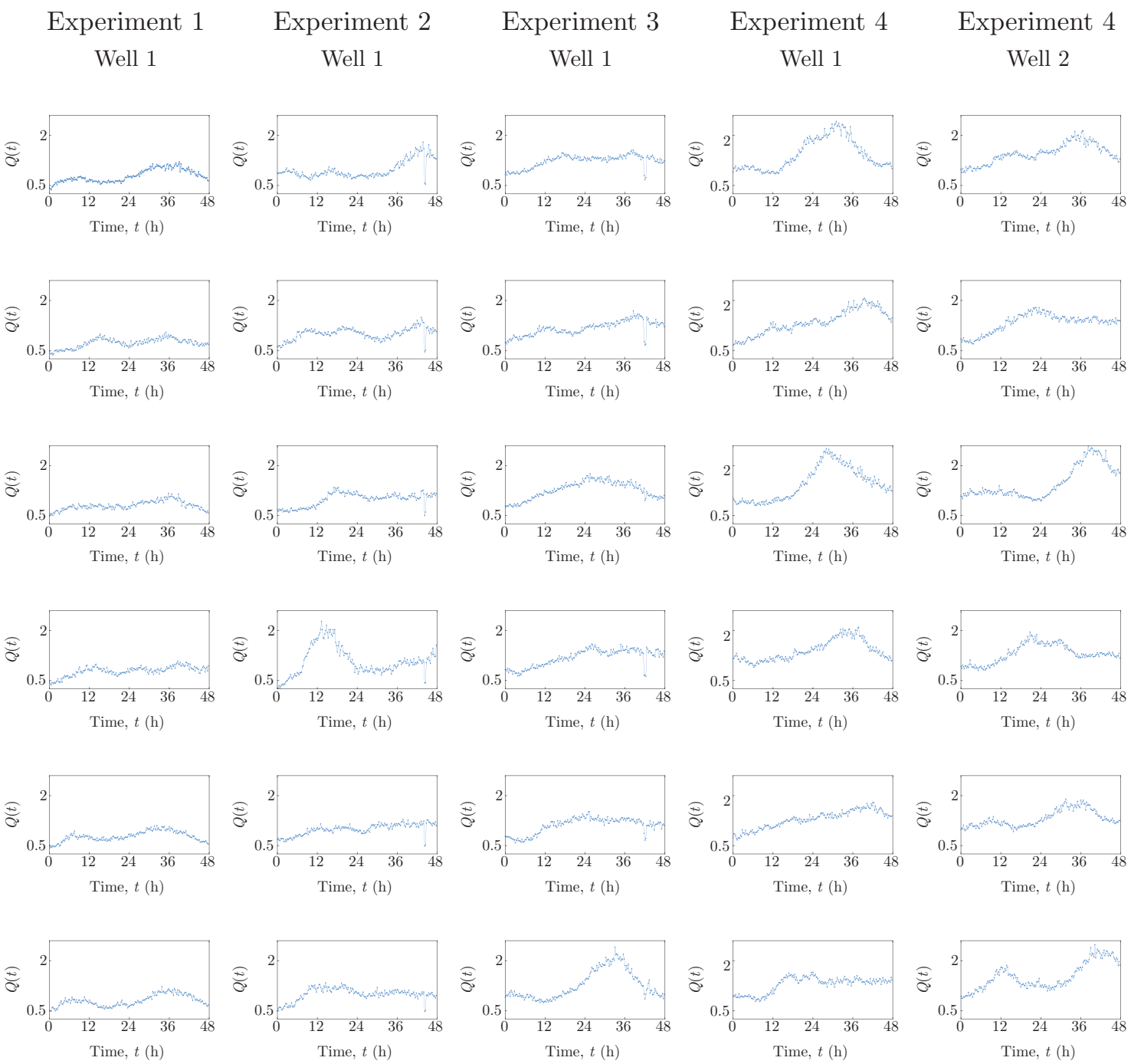


**Figure S9: 1205Lu experimental data.** Ratio $Q(t)$ of the number of cells in G1 to the number of cells in eS/S/G2/M.

# References


[1] Davies MA, Stemke-Hale K, Lin E, Tellez C, Deng W, Gopal YN, et al. Integrated molecular and clinical analysis of AKT activation in metastatic melanoma. Clin Cancer Res. 2009;15:7538–7546.

[2] Hoek KS, Schlegel NC, Brafford P, Sucker A, Ugurel S, Kumar R, et al. Metastatic potential of melanomas defined by specific gene expression profiles with no BRAF signature. Pigment Cell Res. 2006;19:290–302.

[3] Smalley KSM, Contractor R, Haass NK, Kulp AN, Atilla-Gokcumen GE, Williams DS, et al. An organometallic protein kinase inhibitor pharmacologically activates p53 and induces apoptosis in human melanoma cells. Cancer Research. 2007;67:209–217.

[4] Smalley KSM, Contractor R, Haass NK, Lee JT, Nathanson KL, Medina CA, et al. Ki67 expression levels are a better marker of reduced melanoma growth following MEK inhibitor treatment than phospho-ERK levels. Br J Cancer. 2007;96:445–449.

[5] Smalley KSM, Brafford P, Haass NK, Brandner JM, Brown E, Herlyn M. Up-regulated expression of zonula occludens protein-1 in human melanoma associates with N-cadherin and contributes to invasion and adhesion. Am J Pathol. 2005;166:1541–1554.

[6] Sakaue-Sawano A, Kurokawa H, Morimura T, Hanyu A, Hama H, Osawa H, et al. Visualizing spatiotemporal dynamics of multicellular cell-cycle progression. Cell. 2008;132:487–498.

[7] Haass NK, Beaumont KA, Hill DS, Anfosso A, Mrass P, Munoz MA, et al. Real-time cell cycle imaging during melanoma growth, invasion, and drug response. Pigment Cell Melanoma Res. 2014;27:764–776.

[8] Beaumont KA, Anfosso A, Ahmed F, Weninger W, Haass NK. Imaging- and flow cytometry-based analysis of cell position and the cell cycle in 3D melanoma spheroids. J Vis Exp. 2015;106:e53486.

[9] Spoerri L, Beaumont KA, Anfosso A, Haass NK. Real-time cell cycle imaging in a 3D cell culture model of melanoma. Methods Mol Biol. 2017;1612:401–416.

[10] The MathWorks, Inc. Fit curve or surface to data; Accessed February 2019. Available from: https://au.mathworks.com/help/curvefit/fit.html.

[11] The MathWorks, Inc. Solve nonlinear least-squares (nonlinear data-fitting) problems; Accessed February 2019. Available from: https://mathworks.com/help/optim/ug/lsqnonlin.html.

[12] Coleman TF, Li Y. An interior trust region approach for nonlinear minimization subject to bounds. SIAM J Optim. 1996;6:418–445.